Chemical Science

ROYAL SOCIETY OF CHEMISTRY

EDGE ARTICLE

View Article Online
View Journal | View Issue

Cite this: *Chem. Sci.*, 2025, **16**, 14544

All publication charges for this article have been paid for by the Royal Society of Chemistry

Received 25th April 2025
Accepted 4th July 2025

DOI: 10.1039/d5sc03017j

rsc.li/chemical-science

Europium probe binding to serum albumin and α_1-AGP, key importance of configuration, charge and size complementarity†

Huishan Li, [a] Sally Lok-Wan Ng, [a] Dominic J. Black, [b] Wei Han, [a] Robert Pal [b] and David Parker *[a]

Combined luminescence studies and stochastic molecular dynamics simulations have revealed for the first time how cooperative hydrophobic binding and reversible metal ion coordination to protein glutamate residues occurs. A combined experimental and theoretical approach has been used to explain the very different free energies of binding observed between three structurally analogous chiral europium(III) complexes and common variants of serum albumin. In particular, reversible binding of a carboxylate from a glutamate residue was observed; this residue is found in human serum albumin but not the other variants. The binding free energy is exquisitely sensitive to the europium probe structure and charge, and favours complexation of a right handed stereoisomer in the chiral binding pocket. Each process has been visualised by short movies, revealing probe conformational exchange dynamics and the pathway to the protein binding site, on a sub-microsecond timescale.

Introduction

The drugs that bind most strongly to human serum albumin (HSA), possess one or two negatively charged sites and have a complementary size to the different hydrophobic protein binding pockets that allow favourable van der Waals', directed hydrogen bonding, cation–π and π–π interactions to occur. Examples include di-iodosalicylic acid and the dicarboxylate, iodipamide (Fig. 1A), the X-ray contrast agent used in cholangiography that has the highest reported affinity for drug site 1 (DS-1: $\log K = 6.99$).[1] As serum albumin is the ubiquitous transport protein in the body, this protein and its analogues in higher vertebrates have been studied in great detail, for example, BSA (bovine), LSA (rabbit), OSA (sheep), and CSA (goat).[2] These proteins bind with different affinities to the same drug, and it has been noted that BSA is more like HSA than any other variant,[3] and is considered more conformationally rigid.[4] Luminescent probes that bind with selectivity to one or other of the major serum albumin binding sites are rare but important, as they can allow the creation of competitive binding assays for use in drug screening or pharmacokinetic studies.[5,6] Of particular interest are the probes that enhance their emission intensity on binding, especially if the signature emission changes spectral form, allowing ratiometric analysis to be used in quantification.[7] Sporadic reports have emerged detailing probes of the rare earth ions whose emission is enhanced on protein binding. These examples are also of relevance in the behaviour of gadolinium contrast agents with related polydentate ligands, wherein protein binding in serum is intimately associated with both relaxivity enhancement and with the residence and clearance time of the MRI contrast agent in the body, a key issue in defining its toxicity profile.[8] In these studies, HSA has been shown to bind various Gd contrast agents most strongly, compared to other serum albumins.

Early examples of strongly emissive rare earth probes that enhance metal emission on protein binding include a charge neutral terbium DTPA-diamide complex bearing nitroimidazole groups, in which HSA was observed to enhance emission, probably resulting from suppression of oxygen quenching of the chromophore triplet excited state, following protein binding.[9] In addition, certain Eu complexes have been shown to exhibit protein binding in which displacement occurs of a ligand donor or coordinated and/or second sphere water molecules that quench the metal excited state by vibrational energy transfer, leading to emission lifetime and intensity enhancement.[10–12] Of particular interest in this set, are examples in which protein binding (*e.g.* to HSA[13,14] or the important acute phase protein alpha-1-acid glycoprotein (α_1-AGP)[11]) switches on or triggers enhanced circularly polarised luminescence (CPL) from the chiral Eu centre.[15] In this respect, a few well-defined examples of

[a]*Department of Chemistry, Hong Kong Baptist University, Kowloon Tong, 999077, Hong Kong, China. E-mail: davidparker@hkbu.edu.hk*

[b]*Department of Chemistry, Durham University, South Road, Durham DH1 3LE, UK*

† Electronic supplementary information (ESI) available: The synthesis, purification and characterisation of the ligands and their Eu(III) complexes, together with a description of the equipment used for luminescence and CPL measurements and their analysis. Conventional molecular dynamics and metadynamics simulations, trajectory post-processing and data analysis were performed in water (0.15 M NaCl) and relevant references are given. See DOI: https://doi.org/10.1039/d5sc03017j.

the reversible appearance of CPL have been reported, involving a dynamically racemic Eu probe, in which preferred formation of a non-covalently bound diastereomer occurs, 'switching on' the CPL.[11,13,14,16]

The creation of selective CPL probes is beginning to attract increasing attention in solution, thin films and in the solid-state, as the benefits of encoding the 'signature' chiroptical information become more widely appreciated.[17] For example, perovskite nanoparticles have been defined in lanthanide MOFs in which the CPL can be turned on[18] and various examples with chiral catenanes and rotaxanes are emerging, albeit with modest emission dissymmetry factors.[19] Most recently, 'solvent or medium responsive' CPL probes have been reported with highly emissive Eu complexes, allowing the tailoring of CPL sign sequences for possible use in security tag applications.[20] Chiral lanthanide complexes with extended π conjugation for efficient CPL *via* two-photon excitation have also been reported.[21]

Results and discussion

With this background in mind, we have set out to explore the scope and utility of conformationally fluxional complexes of Eu as CPL and ratiometric probes of the local chiral environment. Here, we present remarkable selectivity behaviour in protein binding with three structurally related Eu di-aqua complexes, [EuL$^{1-3}$] (Fig. 1A). By analogy with previous studies, each complex can exist as *Δ* and *Λ* stereoisomers in aqueous solution, in which isomer exchange *via* cooperative arm rotation is likely to be fast on the laboratory timescale. The *S* stereogenic centre in each alanine-derived amide moiety is expected to favour formation of one helical stereoisomer. The local environment places two carboxylate groups *ca.* 15 Å apart, a similar distance to that found between the distal carboxylates in the X-ray contrast agent, iodipamide. The hydrophobic rigid chromophore (*i.e.* the antenna group), can bind to a size-matched protein binding pocket. The Eu complex of L^3 is a monocation; the other two complexes are charge neutral and exhibit varying affinities to proteins with different pI values. For example, the serum albumins have pI values in the range 4.7 to 5.8, whereas α_1-AGP is highly sialylated, and has a pI value of 2.7 to 3.2. With a higher overall negative charge, it tends to former stronger non-covalent complexes with cationic species in solution.

Table 1 Selected photophysical properties of the Eu(III) complexes of L$^{1-3}$ (298 K, H_2O; emission decay rate constant data are given in H_2O and D_2O)

	[EuL^1]	[EuL^2]	[EuL^3]$^+$
λ_{max}/nm	323	337	337
k (H_2O)/ms^{-1}	3.70	3.57	3.75
k (D_2O)/ms^{-1}	1.86	1.62	1.73
q[16]	1.9	2.0	2.0

Photophysical properties of [EuL$^{1-3}$]

Each Eu complex was prepared by standard methods and details are given in the ESI.† The major absorbance band for each Eu complex was rather broad and shifted from 323 to 337 nm from [EuL^1] to [EuL^2]. There is a 20 nm shift between the maximum absorption and excitation wavelengths, suggesting the presence of π–π* and longer wavelength internal charge transfer (ICT) transitions[22] that lead to excitation (Fig. 1 and Table 1). The excitation spectra reveal how the use of 365 nm excitation sources is feasible with such a chromophore. From measurements of the emission lifetime in water and D_2O, the hydration state of each complex was estimated to be two,[23,24] as expected for a heptadentate ligand based on 1,4,7,10-tetraazacyclododecane ('cyclen') that is not very sterically demanding.

Binding to proteins and selected oxyanions

The binding capability of each complex, [EuL$^{1-3}$], towards selected proteins and anions, has been assessed by spectrophotometric titrations and emission lifetime measurements. Binding behaviour was studied with human/bovine albumin, goat and rabbit serum, α-1-acid glycoprotein, and various oxyanions including the three natural phosphorylated amino acids (*O*-P-Ser, Thr and Tyr). Following incremental addition of human serum albumin (HSA), to a solution of [EuL^2] in HEPES buffer (pH 7.4, 298 K, 10 mM), a large enhancement of europium luminescence was observed. A 23-fold increase in the total luminescence intensity was measured following addition of HSA, and a binding constant, $\log K = 6.67$ (12) was estimated by non-linear, iterative least-squares fitting, of the $\Delta J = 2/\Delta J = 1$

Table 2 Binding constant values, $\log K$, and excited state lifetimes, τ, for [EuL^1], [EuL^2] and [EuL^3]$^+$ with added protein (serum)[a] or amino acids.[b] (5 μM, λ_{exc} 340 nm, 10 mM HEPES, pH 7.40)[c]

	[EuL^1]		[EuL^2]		[EuL^3]$^+$	
	τ (ms)	$\log K$	τ (ms)	$\log K$	τ (ms)	$\log K$
HEPES buffer	0.27	—	0.28	—	0.34	—
HSA	0.30	—	0.38	6.67[d]	0.37	5.64
BSA	0.28	—	0.28	—	0.35	5.44
Rabbit serum	0.35	—	0.40	—	0.38	—
Goat serum	0.38	—	0.41	—	0.38	—
α_1-AGP	0.27		0.28		0.44	6.13
O-P-Ser	0.27	—	0.29	4.54	0.35	4.67
O-P-Thr	0.27	—	0.29	4.53	0.36	4.41
O-P-Tyr	0.27	—	0.29	4.72	0.35	4.60
$NaHCO_3$	0.42	3.01	0.42	3.34	0.42	4.40
NH_4OAc	0.33	—	0.32	3.13	0.34	4.42

[a] Human serum albumin and bovine serum albumin (10 μM), α_1-AGP (15 μM). [b] *O*-phospho-L-serine/threonine/tyrosine (1 mM), $NaHCO_3$ (2 mM), ammonium acetate (30 mM). [c] The concentration of the europium complex was determined from the chromophore absorbance using the estimated extinction coefficient. [d] Binding constants were determined by monitoring changes in the intensity of the main hypersensitive $\Delta J = 2$ transition at 614 nm. With added HSA and bicarbonate only, the intensity ratio of this electric dipole-allowed transition to the $\Delta J = 1$ magnetic-dipole allowed transition at 591 nm changed significantly and was also used giving $\log K$ values in reasonable agreement (15%, mean of three replicates) with those estimated from intensity only changes (Fig. 1).

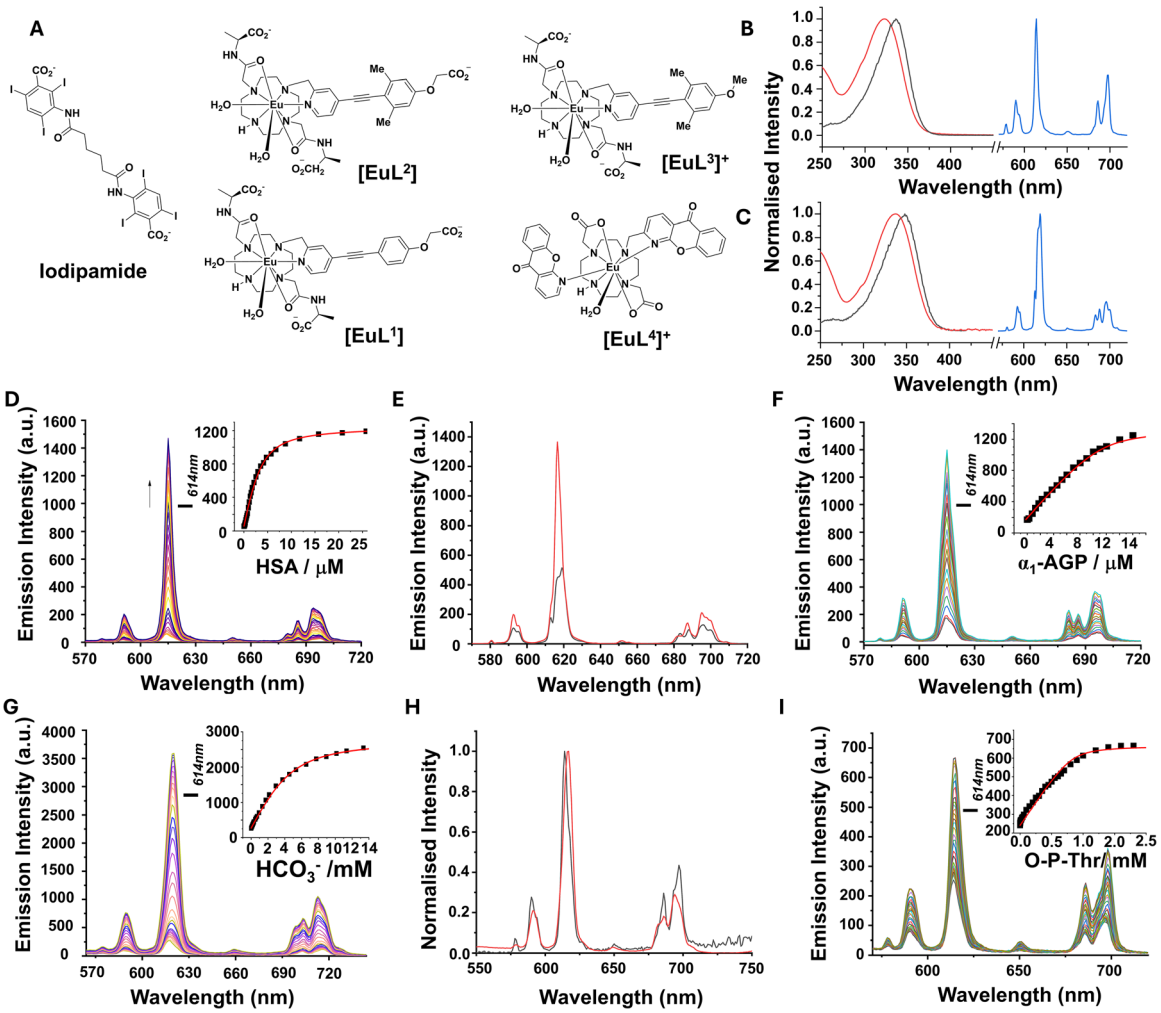

Fig. 1 Photophysical behaviour of the europium complexes with different added proteins and anions. (A) The structures of iodipamide and four europium complexes. Absorption (red), excitation (black), and emission (blue) spectra of: (B) [EuL^1] (H_2O, 298 K, λ_{ex} 330 nm); (C) [EuL^2] (H_2O, 295 K, λ_{ex} 340 nm). (D) Variation of the europium emission spectrum upon binding of HSA to [EuL^2]; ([EuL^2] 5 μM, 10 mM HEPES, pH 7.40, 298 K, λ_{ex} 340 nm). A binding constant ($\log K = 6.83(07)$) was estimated assuming 1 : 1 stoichiometry, (inset). (E) Comparison of the emission spectral fingerprint (right) of [EuL^2] before (black) and after adding HSA (red). (F) Variation of the europium emission spectrum upon binding of α_1-AGP to [EuL^3]$^+$; ([EuL^3]$^+$ 5 μM, 10 mM HEPES, pH 7.40, 298 K, λ_{ex} 340 nm). A binding constant ($\log K = 6.13(05)$) was estimated assuming 1 : 1 stoichiometry, (inset). (G) Variation of the europium emission spectrum (left) on binding HCO_3^- to [EuL^2]; ([EuL^2] 5 μM, 10 mM HEPES, pH 7.40, 298 K, λ_{ex} 340 nm). The binding affinity ($\log K$ 3.47(4)) was fitted assuming 1 : 1 binding stoichiometry. (H) Comparison of emission spectral fingerprints (right) of [EuL^2] before (black) and after adding $NaHCO_3$ (red). (I) Variation of the europium(III) emission profile in [EuL^2] as a function of added *O*-phospho-L-threonine; (left) (5 μM, λ_{exc} 340 nm, 10 mM HEPES buffer, pH 7.40, 298 K, λ_{ex} 340 nm). Insets show the change in the intensity of the emission band at 614 nm with added anion or protein.

intensities assuming a dominant 1 : 1 binding stoichiometry (Fig. 1 and Table 2).

The Eu excited state lifetime was also found to increase from 0.28 to 0.38 ms, and the $\Delta J = 2/\Delta J = 1$ intensity ratio increased by 87% in the HSA bound complex. These changes in emission spectral form, intensity and lifetime strongly suggest that anion binding to the metal occurs, displacing at least one Eu-coordinated water molecule, by more polarisable donor atoms.[13] In contrast, adding BSA to [EuL^2] gave rise to no significant spectral intensity changes and only a 10% increase in emission lifetime. An accurate binding constant could not be determined but a very rough estimate of overall intensity change with BSA gave a $\log K$ value of below 4, at least two orders of magnitude less than with HSA.

When, CSA (caprine/goat) or LSA (rabbit) (in serum form) were added to [EuL^2], no significant changes in either Eu emission spectral form or lifetime were observed (Fig. S1–S3†) and only a reduction in intensity was seen. With [EuL^1], no significant spectral changes were observed when adding any of the serum albumins, suggesting that binding in this case is even weaker and does not involve a change in the primary Eu coordination environment. All that was observed was a spectrum that was identical to the europium aqua complex, with little change in overall emission intensity with added protein, in every case, (Fig. S6†). With the mono-cationic complex, [EuL^3]$^+$ and HSA, a three-fold increase in emission intensity was observed ($\log K = 5.64$) and the lifetime increased by 10%.

No significant spectral or lifetime changes were observed when adding α_1-AGP to [EuL^1] and [EuL^2] (Fig. S2†), notwithstanding its established ability to bind to a lanthanide ion in structurally related complexes to [EuL^1] and [EuL^2].[12] However, with the cationic complex, [EuL^3]$^+$, a seven fold increase in emission intensity and notable changes in emission spectral form were observed, (*e.g.*, the $\Delta J = 2/\Delta J = 1$ ratio increased by 30%, Fig. 1F) and the Eu lifetime increased by 30%. A binding constant of $\log K = 6.13(05)$ was measured, consistent with strong binding into the hydrophobic pocket. This value is slightly higher than that found with the mono-cationic complex [EuL^4]$^+$, ($\log K = 5.82$ (05), in which protein binding was shown to involve displacement of one of the azaxanthone N atoms and a Eu coordinated water molecule; chelation of a Glu-64 side chain carboxylate was implicated.[12]

Emission studies of [EuL^2] with inorganic oxyanions

The binding behaviour of certain oxy-anions was examined, selecting species that have earlier been shown to bind relatively strongly to such di-aqua Eu complexes.[24,25] Very similar changes in the form of the total emission spectrum were observed (*i.e.* an increase of 75% in the $\Delta J = 2/\Delta J = 1$ ratio and similar changes in the fine structure of the $\Delta J = 1$ and 4 manifolds) following addition of either sodium bicarbonate or ammonium acetate to [EuL^2], (Fig. S5† and Table 2), and [EuL^3]$^+$ strongly suggesting that this anion can bind to the lanthanide centre in a similar manner to that seen with [EuL^2] and HSA.

Such behaviour is consistent with formation of a chelated anionic ternary complex, in which a four-membered Eu–O–C–O ring is formed *via* carbonate or carboxylate chelation.[26] The measured affinity constants for bicarbonate with [EuL^1], [EuL^2] and [EuL^3]$^+$ were $\log K = 3.01$, 3.34 and 4.40 respectively, and for binding to acetate, with [EuL^2] and [EuL^3]$^+$, $\log K = 3.13$, and 4.42 (Fig. 1, S5, S7, S8† and Table 2). With [EuL^1], observed changes were much less well-defined, and the binding constant was estimated to be $\log K < 3$. The formation of bidentate chelates between carbonate and acetate and a rare earth metal ion centre has been established by systematic X-ray diffraction and solution-state NMR analyses.[27,28] The higher binding constants with [EuL^3]$^+$ are consistent with the greater gain in free energy arising from coulombic attraction.

In contrast, relatively little change in the emission spectrum of each complex was observed following addition of *O*-P-Ser, *O*-P-Thr or *O*-P-Tyr. The changes in spectral form and overall intensity, however, were sufficiently distinctive to allow binding constants of $\log K = 4.54$, 4.53 and 4.73 to be determined with [EuL^2], for example (Fig. 1). These relatively high $\log K$ values reflect the preference of lanthanide ions for a more polarisable phosphorus oxygen donor, and the slightly higher value with the Tyr example is consistent with its lower free energy of hydration, as it is a slightly more hydrophobic anion. With these phosphorus(v) oxy-anions, chelation does not occur and the oxy-anion binds as a unidentate ligand leaving the axial water intact in these ternary structures.[28]

It has been shown that the ligand field at Eu is exquisitely sensitive to the nature of the axial donor, rather than the equatorial donor[29,30] in such mono-capped square-antiprismatic structures. Such an interpretation agrees with earlier conclusions regarding the constitution and configuration of a variety of ternary anion complexes.[24–27]

Probe and protein structural complementarity

The Eu complex, [EuL^2], bears a somewhat hydrophobic and relatively linear aryl–alkynyl–pyridyl moiety (its chromophore antenna) that may bind to a complementary hydrophobic pocket on the protein. The emission behaviour following protein association is consistent with binding of the complex into a hydrophobic HSA site, namely drug-site 1 (DS-1).[31] Therefore, iodipamide, the di-anion that is known to bind most strongly to DS-1 ($\log K = 6.99$ (04)),[32] was added incrementally to a solution containing [EuL^2] (1.2 μM) and HSA (5 μM) for which $\log K = 6.67$. The emission intensity dropped by a factor of five, and residual Eu luminescence characteristic of the bound complex was observed even with a large excess of added iodipamide, consistent with competitive binding of the probe and iodipamide to DS-1 (Fig. 2B). The equilibrium between the 1 : 1 HSA/[EuL^2] complex and iodipamide under these conditions was characterised by an apparent binding constant, $\log K = 6.03(05)$. Thus, this complex is tuned to assess the relative binding affinity of candidate drugs to HSA in the sub-micromolar range.

A comparison was made of the amino acid sequences in HSA and BSA, by examining the protein data base (PDB) X-ray structures of HSA and BSA, with and without a bound drug: (HSA: 7VRO, 1AO6 (free), 2BXD (warfarin); BSA: 3VO3, 4F5S (free) and 4JK4 (3,5-diodosalicylic acid); 4ORO (naproxen)). The side chain carboxylate groups in Glu-292, Glu-184 or Glu-188 may plausibly be involved in Eu coordination, when [EuL^2] is bound to HSA, as they are relatively close in space to the drug binding site. Critically, Glu-188 and 184 are only found in HSA and are replaced by a Lys or Arg residue and by Thr or Ala, respectively, in the common albumin variants (Fig. S11†).

The next nearest Glu residue in the HSA structure is Glu-153, but it interacts strongly to Arg-256 *via* a stabilising H-bonded salt bridge. With BSA (and by analogy OSA and CSA) the corresponding Glu residue is interacting strongly with a proximate cationic lysine side chain group, (Lys-274 and/or Lys-276). Such favourable intramolecular coulombic and hydrogen bonding interactions are absent in the HSA structures, where Glu-292 and 188/184 are hydrogen bonded to (high energy) water molecules. The displacement of 'high energy' water molecules, following side chain Glu ligation to Eu, may be associated with a favourable free energy change in [EuL^2] binding, as the water molecules return to bulk and a more effective hydrogen bonding environment, *i.e.* such a free energy change is likely to be enthalpically and entropically favourable, considering the local hydration structure.

The binding of [EuL^3]$^+$ to α_1-AGP (*vide supra*) had been shown to be strongest ($\log K$ 6.13) amongst the three Eu probes examined. Chlorpromazine (used to treat severe anxiety and psychotic aggression) binds to this protein with a comparable affinity ($\log K = 6.17$).[33] A competitive titration of the 1 : 1 α_1-AGP/[EuL^3]$^+$ complex with chlorpromazine gave rise to displacement of the Eu probe from the protein adduct (Fig. 2C),

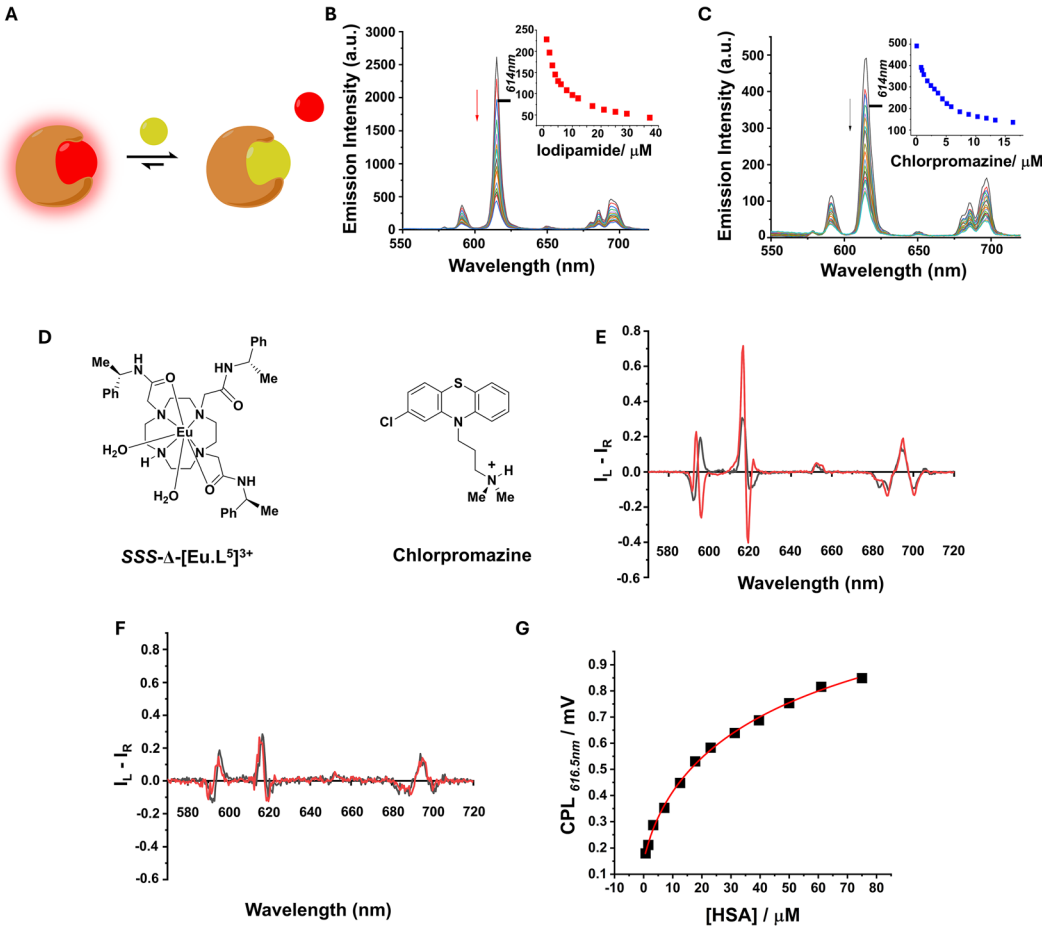

Fig. 2 Competitive drug binding assay and CPL studies of protein binding. (A) Illustration of a competitive assay between drug and the Eu complex-protein bound adduct. (B) Variation of the observed emission (upper) of [EuL^2] (10 μM) in the presence of HSA (5 μM) as a function of iodipamide (298 K, 10 mM HEPES buffer, pH 7.40). (C) Variation of the observed emission (upper) of [EuL^3]$^+$ (10 μM) in the presence of α_1-AGP (5 μM) as a function of [chlorpromazine] (298 K, 10 mM HEPES buffer, pH 7.40). (D) The structure of chlorpromazine and the *SSS-Δ* complex of [EuL^5]$^{3+}$. (E) CPL spectra of [EuL^2] (black) and [EuL^2] following addition of HSA (red) (5 μM complex, 35 μM HSA, λ_{ex} 340 nm, H_2O, 298 K); (F) CPL spectra of [EuL^2] (black) and [EuL^2] following addition of BSA (red) (5 μM complex, 35 μM BSA, λ_{ex} 340 nm, H_2O, 298 K); (G) the binding affinity with HSA (log $K = 6.08(09)$) was estimated by non-linear least squares regression analysis assuming 1 : 1 binding stoichiometry. In the $\Delta J = 1$ manifold, the g(em) values for the di-aqua complex are −0.03 (592), +0.05 (595.5), +0.02 (616), −0.003 (619.5) and in the protein bound adduct, five main transitions appear, slightly shifted in energy and of higher value: −0.03 (591.5), +0.05 (593.5), −0.08 (596) and +0.02 (616.5), −0.02 (619).

and this equilibrium was characterised with an apparent binding constant of log K = 5.90(04). The X-ray structure of chlorpromazine bound to this protein (PDB 3APX) reveals a favourable cation–π interaction between Tyr-36 and the protonated alkylamine group. Both Glu-64 and Glu-92 lie relatively close in space to the guest binding site near the *p*-Cl-phenyl ring, forming a hydrogen bonded array with Arg-90.

Circularly polarised luminescence studies of protein binding

The di-aqua Eu complexes of L^1 and L^2 can undergo relatively fast interconversion of their *Δ* and *Λ* diastereoisomers by cooperative arm rotation. Earlier work with *trans*-di, tri and tetra-substituted chiral amide Eu complexes[27] highlighted the rather weak CPL observed for the *trans*-disubstituted structures bearing a remote stereogenic centre. Relatively weak CPL was observed for the di-aqua complexes of [EuL^1], [EuL^2] and [EuL^3]$^+$, (Fig. S9 and S10†), and no change in the observed CPL was found when adding BSA to either complex. However, binding of [EuL^2] to HSA was accompanied by the appearance of a much stronger CPL signal (Fig. 2), where there were striking changes in the form of both the MD-allowed $\Delta J = 1$ and the ED-allowed hypersensitive $\Delta J = 2$ manifold. A binding constant of log K = 6.08 (09) was estimated by fitting the titration data to a 1 : 1 binding model. The value measured is in reasonable agreement to that obtained by monitoring total emission spectral changes (Fig. 2). The observed sign sequences in the $\Delta J = 1$, 2 and 4 transitions are the same as those found for the di-aqua or carbonate complexes of a structurally characterised *Δ* stereoisomer, the *SSS-Δ* complex of [EuL^5]$^{3+}$.[24,26,34]

Thus, HSA binding of [EuL^2] into the chiral binding pocket of drug site 1, can be hypothesised to favour complexation of the *Δ* complex more strongly than in the unbound complex, in a ternary structure stabilised by concomitant formation of a metal chelate involving the side chain carboxylate of Glu-184 or Glu-188. In this regard, changes in the relative intensity of the $\Delta J = 1$ manifold, notably the sign sequence are very evident,

comparing the di-aqua complex of [EuL^2] *vs.* its HSA-bound species. Such behaviour supports the hypothesis of a change in the Eu coordination environment that perturbs the local ligand field and determines the nature of the magnetic dipole allowed transitions in this manifold. Indeed, the inversion in sign was very apparent for the transition centred at 596 nm (A to E): three transitions were apparent for the protein bound complex, but only two in the aqua complex. By analysing the $\Delta J = 1$ manifold, a second order crystal field coefficient, *i.e.* B_0^2 value of +380(20) cm^{-1} was measured in each case. The absence of change of the ligand field splitting and the fact that only small variations were observed for the *g*(em) values (Fig. 2) strongly suggest that the complex is adopting a square-antiprismatic (SAP) structure in both the di-aqua form and the protein adduct, as it is known that the twisted square antiprismatic (TSAP) isomers have a smaller ligand field splitting in these systems.[30,34] No significant changes were observed in the total emission spectrum when adding either HSA or BSA to [EuL^1], (Fig. S6†) and no CPL could be observed in any example with this europium complex. Furthermore, no change in CPL was observed when adding BSA/CSA or LSA to [EuL^2], (Fig. S9†). With [EuL^3]$^+$, only addition of α_1-AGP gave rise to a modified and more intense CPL signal, (Fig. S10†), and whilst the changes observed were less well-defined than with HSA and [EuL^2], the overall sign sequence was the same, consistent with preferred complexation of the Δ stereoisomer.

Molecular dynamic simulations of [EuL^2]

Molecular dynamics (MD) simulations were conducted to gain structural insight into the details of the binding between [EuL^2] and HSA. The force field developed by Wade *et al.* was employed to model Eu in MD simulations.[35] This force field can maintain the correct coordination geometries of Eu in water without any constraints, thereby enabling simulations of changes to the Eu coordination environment. In this study, the force field was further developed to correctly describe the distance between the europium ion and its ligand donor atoms, replicating the Eu-coordination distances reported experimentally (see ESI†). The simulations with the optimised parameters were carried out in water (0.15 M NaCl) and predicted the preference for a 9-coordinate mono-capped square-antiprismatic coordination geometry (Fig. 3), consistent with structures reported for many similar Eu-complexes.[36] As L^2 is heptadentate, two water molecules from the bulk phase are also found to participate in the coordination shell, with one at one corner of the upper coordination square and the other residing in the axial position (Fig. 3). The prediction of two coordinated water molecules is in accord with the experimentally determined hydration number, (*q* value), of two (Table 1, *vide supra*).

The stochastic simulations revealed that there are two conformational exchange processes occurring with [EuL^2], operating on different timescales. The cooperative rotation of the three ligand arms, involving a switch of the N–C–C–O/N torsional angle of the arms between positive (Δ – clockwise) and negative values (Λ – anticlockwise), occurred on the sub-microsecond timescale (Fig. 3 and Movie A† (**https://doi.org/10.5281/zenodo.15099015**)). With an *S* configuration at C in the alanine moiety, the carboxylate groups at the stereogenic centre prefer to lie away from the π cloud of the pyridine ring: this situation occurs in the Δ isomer but not in the Λ isomer, where the carboxylate is closer to the electron rich aromatic ring. This electrostatic preference of about 2.7 kJ mol^{-1} favours the Δ isomer in [EuL^2] and its congeners (Fig. 3), in agreement with the conclusion of the CPL study. The cooperative ring inversion of the tetra-aza macrocycle, involving the simultaneous sign switch of four N–C–C–N torsional angles on the macrocyclic 12-N-4 ring was much slower, and could not be observed during hundreds of nanoseconds of simulations (Fig. 3). Such behaviour is consistent with a large body of experimental data derived from VT-NMR experiments, that showed that the rate of ring inversion in 12-N-4 coordination complexes of lanthanide ions is relatively slow, with a value of around 50 s^{-1} at ambient temperature.[37]

The free energy profile for ring inversion was further probed through umbrella sampling simulations. As shown in Fig. 3, there is a large barrier of 25.5 kJ mol^{-1} that slows down the rate of ring inversion. The Δ-$\lambda\lambda\lambda\lambda$ isomer, where the values of all the ring N–C–C–N torsion angles are negative (λ, − sign), is lower in free energy than the Δ-$\delta\delta\delta\delta$ isomer (δ, + sign). Thus, in an aqueous solution of [EuL^2] the Δ-$\lambda\lambda\lambda\lambda$ stereoisomer is lower in energy than the Λ-$\delta\delta\delta\delta$ (in 9-coordinate mono-capped square antiprismatic coordination geometries), in accord with the Δ absolute configuration deduced by CPL (Fig. 2).

Molecular dynamics simulations of [EuL^2] binding to HSA

The binding of [EuL^2] to drug-site 1 (DS-1) of HSA was probed through MD simulations. This binding site is located deep inside domain II of HSA but can be accessed from the bulk solution phase *via* a tunnel at the interface of the three domains of HSA (Fig. 3). The metadynamics technique using a funnel-shape restraint (see the ESI† and Fig. 3) was employed to sample the possible binding sites and Eu complex orientation and derive the free energy surface (FES) of the binding process.[38] The restraining funnel is aligned in the direction of the tunnel and covers the entire tunnel. Fig. 3 shows the free energy surface as a function of the distance (d) of [EuL^2] from DS-1 and its relative orientation (θ) with respect to the tunnel. Analysis of the distribution of this binding geometry term (a 2D distribution function, $G\{d,\theta\}$) indicated that [EuL^2] oriented itself in all directions when close to bulk solution but became more constrained when approaching DS-1 (Fig. 3). A sharp energy minimum in narrow ranges of d and θ was identified when [EuL^2] was close to DS-1, indicating that the complex binds to DS-1 in a specific binding geometry (Fig. 3 and Movie B† (**https://doi.org/10.5281/zenodo.15099015**)).

The structures corresponding to this minimum were further analysed (Fig. 3 and Movie C†(**https://doi.org/10.5281/zenodo.15099015**)). The bound complex, [EuL^2], was observed to insert the aryl–alkynyl–pyridyl moiety into DS-1, lean against loop region 289–295, and expose its metal centre to solution and the nearby helix spanning residues 173–206. Various types of interaction between HSA and [EuL^2] were

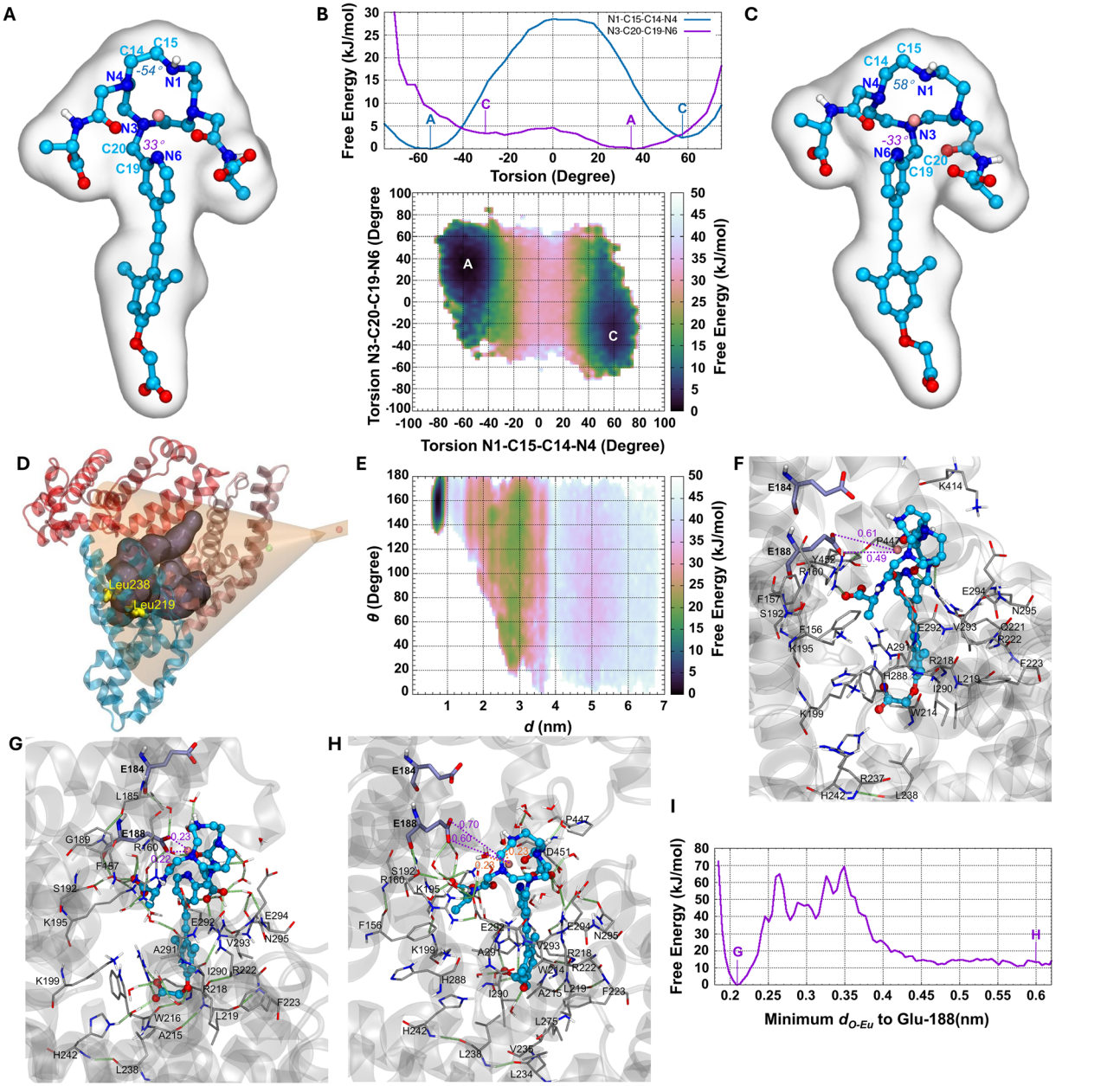

Fig. 3 Molecular dynamics simulations: (A–C) configuration sampling of [EuL^2] in aqueous solvent. (A) Snapshot of [EuL^2] at the global minimum around the Λ-$\lambda\lambda\lambda\lambda$ configuration. (B) 1D-free energy surface (FES) (top) and 2D-FES (bottom) of the N1-C15-C14-N4 torsional angle in the 12-C-4 ring and the N3-C20-C19-N6 torsional angle between the 12-C-4 ring and the pyridine N atom, showing an energy difference of 2.7 kJ mol^{-1} between the two configurations. (C) Snapshot of [EuL^2] at the second lowest minimum around the Λ-$\delta\delta\delta\delta$ configuration. (D–F): Simulation of [EuL^2] binding to HSA. (D) The funnel-shape restraint used for the simulation covering the cavity of DS-1 and the two residues Leu-219/Leu-238 used to define the position of the cavity. (E) 2D-FES $G\{d, \theta\}$ located the bound state in a specific binding geometry prior to metal coordination. (F) Snapshot of the bound state showing the short distance between Eu and Glu-188 carboxylate (d_{O-Eu}) and also the residues within 5 Å of [EuL^2]. Hydrogen bonds are shown as green springs. (G–I) Simulation of Eu-Glu-188 coordination. (G) Snapshot of the lowest energy state showing the bidentate coordination of [EuL^2]-Glu-188 at 0.22–0.23 nm (2.2–2.3 Å). (H) Snapshot of the Eu coordination state with two water molecules at 0.23 nm (2.3 Å) before being displaced by the carboxylate oxygens of Glu-188. (I) 1D-FES of the metal coordination process showing a 13.8 kJ mol^{-1} energy difference between the states shown in G and H. All non-polar hydrogens in simulation snapshots are omitted for clarity.

observed, including favourable electrostatic interactions between Arg-160/Arg-222 and the carboxylate groups of the two alanine-derived arms and between Lys-195/Lys-199/Arg-218 and the single carboxylate group of the chromophore moiety. In addition, there is a cation–π interaction between Arg-222 and the electron rich aryl ring (substituted by an ether oxygen and two methyl groups). Furthermore, favourable hydrophobic interactions occur between Leu-219/Ile-290/Val-293 and the two phenyl ring methyl groups.

Intriguingly, Glu-188 in helix 289–295 was found in proximity to the metal centre of [EuL^2]. The distance between carboxyl oxygen atoms of Glu-188 and Eu fluctuated between

0.4 nm and 1.0 nm, indicating that although the sidechain of Glu-188 remained flexible, it had the potential to coordinate with Eu. However, the coordination of this sidechain with Eu was not observed at first, presumably because of the high energy barrier to replacement of water ligands in the coordination shell of Eu, that could not be overcome during the funnel metadynamics sampling process describing the overall positions and orientations of [EuL^2]. The standard free energy of formation of this bound structure was calculated to be 25.8 kJ mol^{-1}, corresponding to $\log K = 4.50$, considerably smaller than the experimental value ($\log K = 6.67$). Therefore, the bound structure observed here can be considered to represent an intermediate state, before the coordination between Eu and HSA takes place with displacement of the two Eu-bound water molecules.

Therefore, starting with the bound structure, another stochastic metadynamics simulation was conducted to probe the free energy surface for coordination of Glu-188 and [EuL^2]. In this simulation, the distance (d_{O-Eu}) between the carboxylate oxygen and Eu and the water coordination number were employed as collective variables to enhance sampling. The resulting FES exhibits a flat minimum at $d_{O-Eu} > 0.4$ nm, consistent with the results from the funnel metadynamics simulation, and a sharp minimum was located around $d_{O-Eu} = 0.22$ nm, consistent with direct coordination of Glu-188 to Eu (Fig. 3). The two minima were separated by a barrier over 50 kJ mol^{-1}, in accord with the energy barriers found for dissociative water exchange at a rare earth metal centre in complexes with charge neutral donor atoms.[37]

Both monodentate and bidentate coordination modes were observed. The latter occurred more often, consistent with their occurrence in related X-ray structural studies, studying binding of acetate to diaqua-lanthanide complexes.[24,26] The coordination of Glu-188 with Eu further lowered the free energy by 13.8 kJ mol^{-1}, enhancing the affinity of [EuL^2] for HSA. Considering both initial binding and subsequent coordination, the overall affinity of [EuL^2] for HSA, based on the calculation here, is estimated to be $\log K = 4.50 + 2.40 = 6.90$, which agrees fairly well with the experimental result (6.67) from the luminescence titration.

Conclusions

The CPL studies have revealed and MD simulations confirmed and added detailed stereochemical information concerning the nature of the remarkably selective and strong protein interaction between drug site 1 in HSA and [EuL^2], and, by analogy between [EuL^3]$^+$ and α_1-AGP. In each case, both charge and size complementarity are very important, and the combination of favourable hydrophobic binding and reversible metal-coordination to a Glu residue explains the very strong binding free energy. Indeed, these probes offer the opportunity to be used in competitive assays for drugs that strongly interact with the given protein binding site and suggest that such an approach offers much scope in designing high affinity antagonists in a more general sense, *e.g.* for drug discovery use.

At the pocket entrance to drug site-1 in HSA, Lys-195/199 and Arg-218 and 222 are found; in the species variants, these residues are also either Lys or Arg. At the base of DS-1, His-242, Arg-257 and Tyr-150 are present in HSA and in all variants (Fig. S11†).The overall free energy of protein binding with the Eu complexes is thus made up of three major contributions: the first involves favourable electrostatic interactions of the two alanine carboxylate groups and the basal carboxylate on the aryl ring in the complex to the proximate Lys, Arg and His residues in the protein (Fig. 3 and Movie C† (**https://doi.org/10.5281/zenodo.15099015**)); the second is a classical hydrophobic effect, enhanced by a cation–π interaction between Arg-222 and the electron rich aryl ring, where the binding pocket and the chromophore aromatic moiety are size-matched; the third involves reversible metal coordination of a proximate Glu carboxylate side chain, *i.e.* Glu-188 in HSA and Glu-64 with a_1-AGP, displacing Eu-bound water molecules, accompanied by the return to bulk of 'high energy' water molecules that occupy the drug binding site or are hydrogen-bonded to the Glu residue side chain. Such an interaction has been hypothesised to occur in the past for a variety of diaqua lanthanide coordination complexes, notably gadolinium.[39]

This selective protein binding behaviour is not exhibited by [EuL^1]. It lacks two methyl groups on the peripheral aryl ring and has a relatively weak affinity for every serum albumin studied and for α_1-AGP. This very striking size complementarity between the drug-site 1 binding pocket and the aryl–alkynyl–pyridyl moiety is remarkably finely tuned, in a manner that has no obvious precedent. Given that protein–ligand binding rate constants for association are typically of the order of 10^5 to 10^6 M^{-1} s^{-1},[40] then the binding of [EuL^2] to HSA and of [EuL^3]$^+$ to α_1-AGP is likely to be associated with a dissociation rate of 10^{-2} to 10^0 s^{-1}, *i.e.* slow on the Eu emission timescale. A tentative explanation for the weaker binding of [EuL^1] in each case, and the invisible Eu CPL, can then be traced to a faster dissociation rate and a lower free energy barrier to dissociation, owing to the smaller steric demand of the aryl moiety in this Eu complex. Indeed, the nearest residue to the aryl *ortho* positions (Me *vs.* H) are relatively bulky hydrophobic residues *i.e.* Leu-219/Ile-290/Val-293 residues (Movie C† (**https://doi.org/10.5281/zenodo.15099015**)). Thus, the dramatic impact of Me/H substitution in the aryl ring in these complexes may tentatively be ascribed both to a higher free energy of binding, when more favourable non-bonding interactions involving the methyl groups on the phenyl ring can occur, and to a concomitant larger steric barrier for dissociation, (*i.e.* for [EuL^2]), that slows down the rate of dissociation of the more bulky complex from its protein bound state.

Data availability

The data supporting this article have been included as part of the ESI.†

Author contributions

The manuscript was written by DP with contributions from each author; HL carried out the syntheses and characterisation, and the measurements of binding and rate constants at steady state; DB and RP undertook the CPL measurements in Durham; Sally Ng undertook the molecular dynamics studies and stochastic metadynamics simulations under direction from HW.

Conflicts of interest

There are no conflicts to declare.

Acknowledgements

DP thanks the Hong Kong Jockey Club Charities Trust for equipment support and the Hong Kong Government and Hong Kong Baptist University for support under the Global STEM Professorship scheme.

Notes and references

1 F. Yang, Y. Zhang and H. Liang, *Int. J. Mol. Sci.*, 2015, **15**, 3580–3595.
2 P. Pongprayoon, N. Kuntip, T. Suwanasopee, D. Jattawa, J. Miranitranon, D. Japrung and S. Koonawootrittriron, *J. Biomol. Struct. Dyn.*, 2025, **43**, 2772–2780.
3 D. A. Belinskaia, P. A. Voronina, V. I. Shmurak, R. O. Jenkins and N. V. Goncharov, *Int. J. Mol. Sci.*, 2021, **22**, 10318.
4 S. Ketrat, D. Japrung and P. Pongprayoon, *J. Mol. Graphics Modell.*, 2020, **98**, 107601.
5 G. D. Li, C. Wu, D. L. Ma and C. H. Leung, *TrAC, Trends Anal. Chem.*, 2021, **139**, 116270.
6 R. Jouclas, S. Laine, S. V. Eliseeva, J. Mandel, F. Szeremeta, P. Retailleau, J. He, J.-F. Gallard, A. Pallier, C. Bonnet, S. Petoud, P. Durand and E. Toth, *Angew. Chem., Int. Ed.*, 2024, **63**, e202317728.
7 D. Parker, J. D. Fradgley and K.-L. Wong, *Chem. Soc. Rev.*, 2021, **50**, 8193–8213.
8 H. B. Eldredge, M. Spiller, J. M. Chasse, M. T. Greenwood and P. Caravan, *Invest. Radiol.*, 2006, **41**, 229–243.
9 X. Wang, X. Wang, Y. Wang and Z. Guo, *Chem. Commun.*, 2011, **47**, 8127–8129.
10 S. Dasari and A. K. Patra, *Dalton Trans.*, 2015, **44**, 19844–19855.
11 S. Shuvaev, E. A. Suturina, K. Mason and D. Parker, *Chem. Sci.*, 2018, **9**, 2996–3003.
12 H. Li, D. Parker, J.-X. Zhang and H. Li, *J. Lumin.*, 2023, **60**, 119852.
13 R. Carr, L. Di Bari, S. Lo Piano, D. Parker, R. D. Peacock and J. M. Sanderson, *Dalton Trans.*, 2012, **41**, 13154–13158.
14 S. Shuvaev, R. Pal and D. Parker, *Chem. Commun.*, 2017, **53**, 6724–6727.
15 Y. Kitagawa, M. Tsurui and Y. Hasegawa, *ACS Omega*, 2020, **5**, 3786–3791.
16 Y. Okayasu, K. Wakabayashi and J. Yuasa, *Inorg. Chem.*, 2022, **61**, 15108–15115.
17 D. F. De Rosa, P. Stachelek, D. J. Black and R. Pal, *Nat. Commun.*, 2023, **14**, 1537.
18 C. Zhang, Z.-S. Li, X.-Y. Dang, Y.-Y. Nin and Y.-Y. Zang, *Adv. Mater.*, 2022, **34**, 2109496.
19 Y. Wang, J. Gong, X. Wang, W.-J. Li, X.-Q. Wang, X. He, W. Wang and H.-B. Yang, *Angew Chem. Int. Ed. Engl.*, 2022, **61**, e202210542.
20 D. F. De Rosa, M. Starck, R. Pal and D. Parker, *Chem.–Eur. J.*, 2024, **30**, e2023322.
21 O. G. Willis, F. Petri, D. F. De Rosa, A. Mandoli, R. Pal, F. Zinna and L. Di Bari, *J. Am. Chem. Soc.*, 2023, **145**, 25170–25176.
22 M. Soulié, F. Latzko, E. Bourrier, V. Placide, S. J. Butler, R. Pal, J. W. Walton, P. L. Baldeck, B. Le Guennier, C. Andraud, J. M. Zwier, L. Lamarque, D. Parker and O. Maury, *Chem.–Eur. J.*, 2014, **20**, 8636–8646.
23 A. Beeby, I. M. Clarkson, R. S. Dickins, S. Faulkner, D. Parker, L. Royle, A. S. de Sousa, J. A. G. Williams and M. Woods, *J. Chem. Soc., Perkin Trans. 2*, 1999, 493–504.
24 J. I. Bruce, R. S. Dickins, L. J. Govenlock, T. Gunnlaugsson, S. Lopinski, M. P. Lowe, D. Parker, R. D. Peacock, J. J. B. Perry, S. Aime and M. Botta, *J. Am. Chem. Soc.*, 2000, **122**, 9674–9684.
25 S. J. Butler and D. Parker, *Chem. Soc. Rev.*, 2013, **42**, 1652–1666.
26 R. S. Dickins, S. Aime, A. S. Batsanov, A. Beeby, M. Botta, J. I. Bruce, J. A. K. Howard, C. S. Love, D. Parker, R. D. Peacock and H. Puschmann, *J. Am. Chem. Soc.*, 2002, **124**, 12697–12705.
27 S. E. Bodman and S. J. Butler, *Chem. Sci.*, 2021, **12**, 2716–2734.
28 P. Atkinson, Y. Bretonniere, G. Muller and D. Parker, *Helv. Chim. Acta*, 2005, **88**, 391–405.
29 L. Di Bari, G. Pintacuda, P. Salvadori, R. S. Dickins and D. Parker, *J. Am. Chem. Soc.*, 2000, **122**, 9257–9264.
30 D. Parker, E. A. Suturina, I. Kuprov and N. F. Chilton, *Acc. Chem. Res.*, 2020, **53**, 1520–1534.
31 I. Petitpas, A. A. Bhattacharya, S. Twine, M. East and S. Curry, *J. Biol. Chem.*, 2001, **276**, 22804–22809.
32 S. Ashraf, H. Qaiser, S. Tariq, A. Khalid, H. Makeen, H. A. Alhazmi and Z. Ul-Haq, *Curr. Res. Struct. Biol.*, 2023, **6**, 100114.
33 C. Bi, A. Jackson, J. Vargas-Badilla, R. Li, G. Rada, J. Anguizola, E. Pfaunmiller and D. S. Hage, *J. Chromatogr. B*, 2016, **1021**, 188–196.
34 J. I. Bruce, D. Parker, R. D. Peacock and S. Lopinski, *Chirality*, 2002, **14**, 562–567.
35 D. B. Kokh, M. Amaral, J. Bomke, U. Gradler, D. Musli, H.-P. Buchstaller, M. K. Dreyer, M. Frech, M. Lowinski, F. Vallee, M. Bianciotto, A. Rak and R. C. Wade, *J. Chem. Theory Comput.*, 2018, **14**, 3859–3869.
36 J. Zhang, L. Dai, A. M. Webster, W. T. K. Chan, L. E. Mackenzie, R. Pal, S. L. Cobb and G.-L. Law, *Angew Chem. Int. Ed. Engl.*, 2021, **60**, 1004–1010.
37 D. Parker, R. S. Dickins, H. Puschmann, C. Crossland and J. A. K. Howard, *Chem. Rev.*, 2002, **102**, 1977–2010.
38 S. Raniolo and V. Limongelli, *Nat. Protoc.*, 2020, **15**, 2837–2866.
39 S. Aime, E. Gianolio, E. Terreno, G. B. Giovenzana, R. Pagliarin, M. Sisti, G. Palmisano, M. Botta, M. P. Lowe and D. Parker, *J. Biol. Inorg. Chem.*, 2001, **5**, 488–497.
40 V. Maes, Y. Engelborghs, J. Hoebeke, Y. Maras and A. Vercruysse, *Mol. Pharmacol.*, 1982, **21**, 100–107.